

Efficient Recursive Convolution Schemes for the Accurate FDTD Modeling of Graphene Interband Contribution via Complex Conjugate Pairs

S. A. Amanatiadis¹, T. T. Zygidis², T. Ohtani³, Y. Kanai⁴, and N. V. Kantartzis¹

¹Department of Electrical and Computer Engineering, Aristotle University of Thessaloniki, 54124 Thessaloniki, Greece

²Department of Electrical and Computer Engineering, University of Western Macedonia, 50131 Kozani, Greece

³Private Researcher, Asahikawa 070-0841, Japan

⁴Department of Information and Electronics Engineering, Niigata Institute of Technology, Kashiwazaki 945-1195, Japan

The accurate time-domain numerical modeling of graphene surface conductivity due to the interband contribution is presented in this paper. Initially, the lower frequency limit for the interband conductivity inclusion is studied, highlighting that even in the far-infrared regime it should not be ignored. Then, a precise vector-fitting technique is utilized to decompose the analytical conductivity function into complex conjugate pairs. Every pair is connected to a complex surface current, while the frequency dispersion is evaluated via a proper recursive convolution scheme. Finally, a straightforward algebraic manipulation is conducted to eliminate the complex terms from the update equations of the electromagnetic components, concerning the finite-difference time-domain (FDTD) algorithm. The precision and efficiency of the proposed methodology are thoroughly validated by comparing the numerically extracted surface wave propagation characteristics to those obtained in terms of analytical expressions.

Index Terms—Graphene, recursive convolution method, surface current, surface wave, time-domain, vector-fitting.

I. INTRODUCTION

THE rapid evolution of communications shifts the frequency regime towards the THz scale owing to the increased requirements for spectral bandwidth [1]. To this aim, advanced materials are employed, such as graphene, which exhibits an impressive electromagnetic response, despite its negligible thickness. Specifically, its ability to support strongly confined surface plasmon polariton (SPP) waves facilitates the design of various promising THz devices, like nano-antennas [2]–[4] and plasmonic filters [5], [6]. Indeed, the investigation and optimization of such advanced components is not viable through analytical approaches; therefore, properly adjusted numerical techniques are required, such as the popular finite-difference time-domain (FDTD) algorithm.

The efficient incorporation of graphene in the FDTD method is, nowadays, a straightforward procedure since it can be efficiently modeled as an equivalent surface current. The latter is imported to the conventional update algorithm either via the direct connection to the electric field [7] or using a split technique for the tangential magnetic components to enforce the corresponding boundary condition [8]. Moreover, the far-infrared dominant intraband conductivity term follows a standard Debye frequency dispersion, and various well-known schemes, like the auxiliary differential equation (ADE) and the recursive convolution method (RCM), have been effectively employed. Nevertheless, the transient numerical modeling of graphene beyond mid-infrared frequencies remains a challenging task, since non-trivial interband electron transitions dominate its conductivity. During the previous years, several interesting modifications have been discussed for the FDTD method. In particular, the Padé polynomial approximation [9]

and its enhancement using an iterative procedure [10] have been proposed, while some promising results have been acquired via the complex conjugate pair modeling [11].

In this paper, the latter scheme is extended to a rigorous implementation that requires the minimum number of graphene terms, while the storage of previous time-steps is effectively avoided. As a first step, the significance of the interband term is investigated for the accurate graphene modeling, even at the far-infrared regime, especially for low chemical potential values. Additionally, the introduction of the two-dimensional (2D) material in the conventional FDTD scheme is achieved by utilizing one complex surface current for each complex-conjugate pair, whereas a robust recursive convolution method (RCM) is applied. Then, an appropriate algebraic manipulation is realized to import the aforementioned complex surface current into the real-valued update equations of the electric field. Finally, the proposed scheme is verified, in terms of accuracy and efficiency, by means of a thorough comparison of the numerically calculated surface wave propagation characteristics to those acquired through theoretical formulas.

II. THEORETICAL FORMULATION

A. Graphene Surface Conductivity

Throughout our work, graphene is considered as an infinitely thin material, characterized via its surface conductivity $\sigma_{\text{gr}}(\omega, \mu_c, \Gamma, T)$, where ω is the frequency, μ_c and Γ are the chemical potential, and scattering rate, respectively, and T is the temperature. The surface conductivity expression is derived using the Kubo formula, where two terms are distinguished, based on the electron transitions [12]

$$\sigma_{\text{intra}}(\omega) = \frac{A\mu_c}{j\omega + 2\Gamma}, \quad (1a)$$

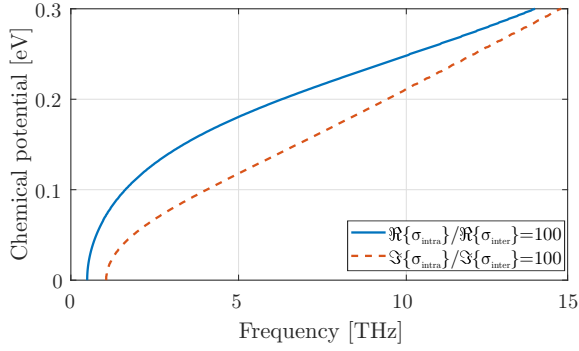


Fig. 1. Frequency limit for 1% error, when only the intraband term is used for the modeling of graphene.

$$\sigma_{\text{inter}}(\omega) = \int_0^{\infty} A_E(E) \frac{j\omega + 2\Gamma}{(j\omega + 2\Gamma)^2 + 4(E/\hbar)^2} dE, \quad (1b)$$

with A_{μ_c} a frequency independent term, \hbar the reduced Planck constant and $A_E(E)$ defined as

$$A_E(E) = |q_e|^2 \frac{f_d(-E) - f_d(E)}{\pi \hbar^2}, \quad (2)$$

for q_e the electron charge and $f_d(\varepsilon)$ the Fermi-Dirac distribution. The conductivity term in (1a) is the intraband one and it is dominant up to low THz frequencies. Moreover, it is described by a simple Debye model; thus, its time-domain modeling is, nowadays, trivial. Conversely, the interband term of (1b) can not be interpreted through a well-known dispersion function, such as a Debye, Lorentz, or Drude model.

As already mentioned, the interband term is generally deemed negligible at low THz frequencies. However, this is not accurate, especially for low chemical potential values, as illustrated in Fig. 1. Herein, the frequency limit is computed at the point where $\sigma_{\text{intra}}/\sigma_{\text{inter}} = 100$, both for the real and imaginary part. The value of 100 is arbitrarily selected and corresponds to the upper limit for approximately 1% error of the graphene conductivity when the interband term is neglected. Indeed, the requirement for a decreased error reduces considerably this upper limit. Therefore, it is evident, now, that the incorporation of the interband term is crucial, even at the far-infrared regime for the precise modeling of graphene. As an indicative example, the defined limit for $\mu_c = 0.1$ eV is approximately at 1 THz.

B. Interband Conductivity Approximation

It is apparent that (1b) can not be described by any well-known dispersion model; consequently, its numerical modeling in a transient solver is proven to be demanding. For this reason, a vector-fitting technique [13] is applied to decompose the surface conductivity into N pairs of complex-conjugate Debye components in the form of

$$\sigma_{\text{inter}}(\omega) \approx \sum_{p=1}^N \left(\frac{c_p}{j\omega + \alpha_p} + \frac{c_p^*}{j\omega + \alpha_p^*} \right). \quad (3)$$

The performance of this vector-fitting algorithm is validated using the realistic $\mu_c = 0.1$ eV and $\Gamma = 0.11$ meV graphene

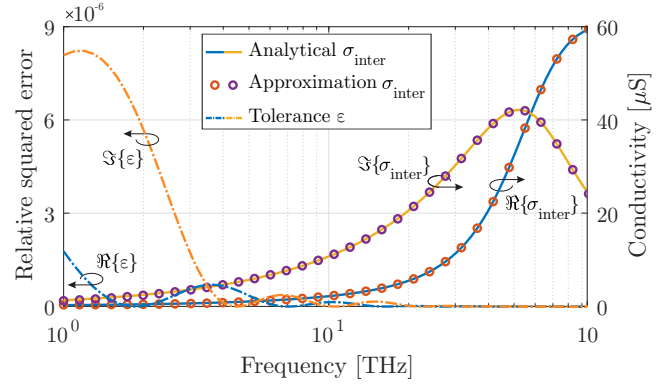


Fig. 2. Graphene surface conductivity due to the interband contribution and its approximation through the vector-fitting technique.

TABLE I
GRAPHENE INTERBAND CONDUCTIVITY COMPONENTS
USING THE VECTOR-FITTING TECHNIQUE

Component	α_p	c_p
1	5.08×10^{14}	1.21×10^{10}
2	$(2.42 \pm j3.05) \times 10^{14}$	$(0.12 \pm j8.66) \times 10^9$
3	4.69×10^{13}	7.60×10^7
4	2.84×10^{17}	1.74×10^{13}

parameters. The approximation of the original function, for the desired error tolerance of 10^{-5} , is depicted in Fig. 2, proving a remarkable behavior. Moreover, all the α_p and c_p values of the required Debye-like components are summarized in Table I. Evidently two different types of functions can be evaluated, either real-valued (components 1, 3, and 4) or a pair of complex-conjugate (component 2). It is, also, worth mentioning that the 4th component is almost 3 orders of magnitude larger than the maximum frequency, namely 100 THz; hence, it can be estimated via the constant conductivity $c_4/\alpha_4 = 61.26 \mu\text{S}$, since $\alpha_4 \gg j\omega$. Interestingly, this value is almost equal to graphene's constant conductivity at optical frequencies [12].

C. Graphene Modeling in the FDTD Method

The efficient modeling of graphene in the FDTD algorithm is accomplished by treating it as the equivalent surface current $\vec{J}_{\text{gr}} = \sigma_{\text{gr}}(\omega)\vec{E}$, separated into the intraband and the interband conductivity mechanisms, as

$$\vec{J}_{\text{gr}} = \vec{J}_{\text{gr,intra}} + \vec{J}_{\text{gr,inter}} = \vec{J}_{\text{gr,intra}} + \sum_{p=1}^N \vec{J}_p, \quad (4)$$

where \vec{J}_p corresponds to the extracted components of the vector-fitting technique. All the surface current vectors are located at an identical position to the electric ones of the Yee cell, as demonstrated in Fig. 3, considering graphene at the xz -plane. Moreover, the FDTD implementation for the intraband term is an easy procedure [7], while the real-valued components of Table I can be handled equivalently, as they are described by the standard Debye function. Therefore, the challenge is the appropriate determination of the conductivity components due to the complex-conjugate pairs.

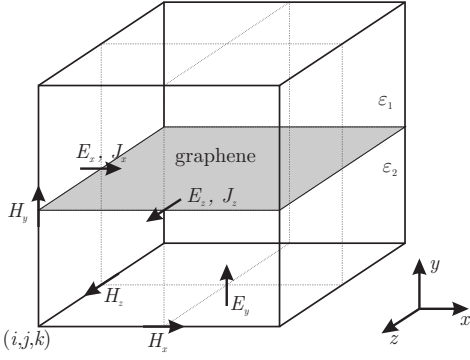


Fig. 3. The modified Yee cell including the surface current components for the incorporation of graphene at the xz -plane.

Initially, the time-domain transition is conducted for the $\vec{J}_p(\omega)$ components via the inverse Fourier transformation as

$$\vec{J}_p(\omega) = \sigma_p(\omega) \vec{E}(\omega) \xrightarrow{\text{IFT}} \vec{J}_p(t) = \sigma_p(t) * \vec{E}(t), \quad (5)$$

where σ_p is the p complex-conjugate component of (3), i.e.

$$\vec{J}_p(t) = \left(c_p e^{-\alpha_p t} + c_p^* e^{-\alpha_p^* t} \right) * \vec{E}(t). \quad (6)$$

Then, the Euler formula is employed for the exponential terms and a straightforward algebraic manipulation is conducted

$$\vec{J}_p = \left(2\Re\{c_p\} \Re\{e^{-\alpha_p t}\} + 2\Im\{c_p\} \Im\{e^{-\alpha_p t}\} \right) * \vec{E}, \quad (7)$$

with $\Re\{\cdot\}$ and $\Im\{\cdot\}$ indicating the real and imaginary parts, respectively. Interestingly, the complex values are eliminated, which facilitates the application of a standard RCM technique for each term in (7). However, we propose an additional simplification to efficiently minimize the required surface current calculations, stemming from the symmetry of (7). In particular, the complex surface current $\vec{J}_{c,p}$ is introduced

$$\vec{J}_{c,p}(t) = e^{-\alpha_p t} * \vec{E}(t), \quad (8)$$

where, only the α_p value is used for the p complex-conjugate component. Next, the the RCM is calculated in terms of

$$J_{c,p}^{n+\frac{1}{2}} = J_{c,p}^{n-\frac{1}{2}} e^{\alpha_p t} + E^n \Delta t. \quad (9)$$

Based on the above aspects, the contribution of the omitted c_p value and the elimination of the complex values is realized directly in the electric field update equation to derive

$$E^{n+1} = E^n + \frac{\Delta t}{\epsilon_0} \nabla \times \vec{H}^{n+\frac{1}{2}} + \frac{\Delta t}{\epsilon_0 \Delta y} \sum_{p=1}^N \left(2\Re\{c_p\} \Re\{J_{c,p}^{n+\frac{1}{2}}\} + 2\Im\{c_p\} \Im\{J_{c,p}^{n+\frac{1}{2}}\} \right). \quad (10)$$

Note that the modified update expression for the electric field results from Ampere's integral law [7]. It is, finally, important to stress that the entire procedure requires one complex surface current for each complex-conjugate pair, while the leapfrog procedure advances without the requirement of any previously stored value.

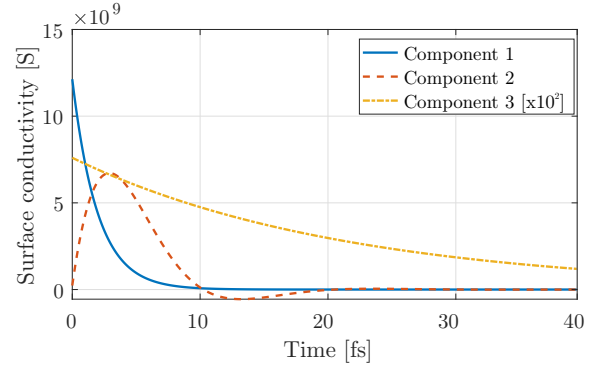


Fig. 4. Interband conductivity components in the time-domain.

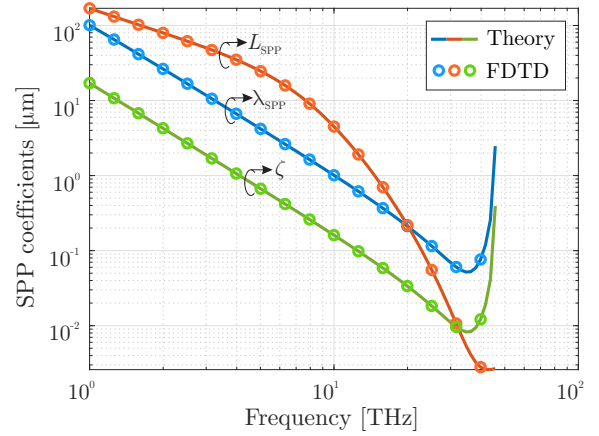


Fig. 5. Comparison of surface wave propagation properties evaluated theoretically and by means of the proposed FDTD technique.

III. NUMERICAL VALIDATION

The validity of our scheme is examined through the numerical evaluation of the SPP propagation properties on graphene and their comparison to their theoretical values

$$\lambda_{\text{SPP}} = \frac{2\pi}{\Re\{k_\rho\}}, \quad L_{\text{SPP}} = \frac{0.5}{\Im\{k_\rho^*\}}, \quad \zeta = \frac{1}{\Re\left\{\sqrt{k_\rho^2 - k_0^2}\right\}}, \quad (11)$$

with k_0 the free-space wavenumber, k_ρ defined as

$$k_\rho = k_0 \sqrt{1 - 4/(\sigma_{\text{gr}} \eta_0)^2}, \quad (12)$$

and η_0 the free-space wave-impedance. Observe that σ_{gr} includes both intraband and interband contributions.

The characteristics of graphene are selected, as previously, to be $\mu_c = 0.1$ eV and $\Gamma = 0.11$ meV, while the conductivity components of Table I in the time-domain are plotted in Fig. 4. It can be detected that the purely real ones present an exponential decay in contrast to the oscillation pattern of the complex-conjugate pair which is, also, real-valued. Component 4 has been omitted since it corresponds to the constant conductivity value $61.26 \mu\text{S}$, as explained in Section II-B.

The FDTD domain is discretized into $200 \times 100 \times 200$ cubic cells, while three different setups are considered to cover the entire frequency range. In particular, the cell-size Δ is selected $1 \mu\text{m}$, $0.1 \mu\text{m}$, and 10 nm , leading to a stable time-step Δt of 1.9 fs , 0.19 fs , and 19 as , correspondingly. Furthermore, open

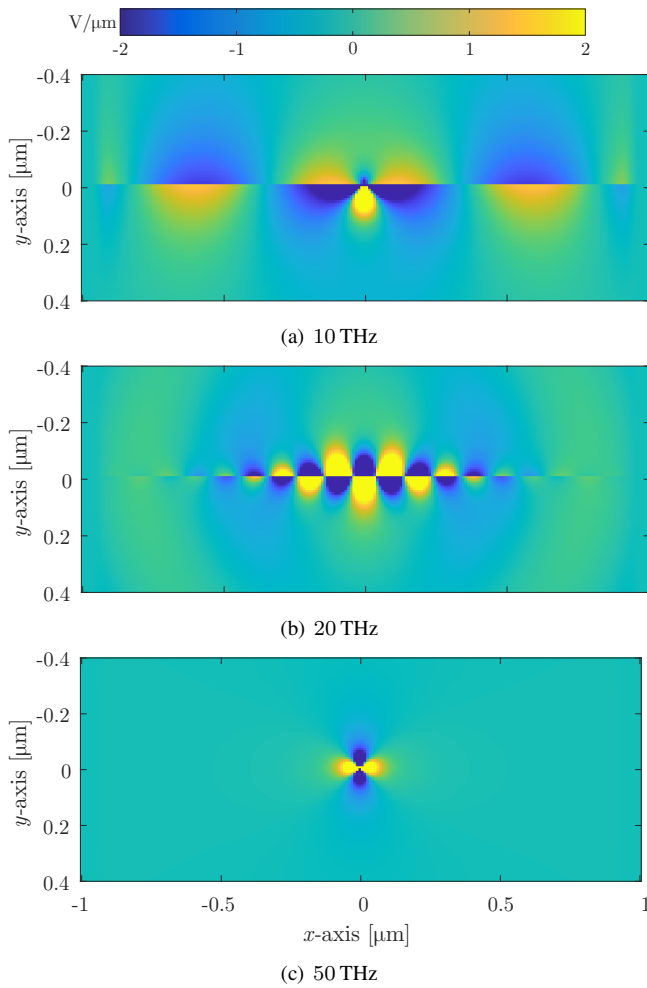


Fig. 6. Electric field distribution of the normal, to graphene, vector at different frequencies.

boundaries are terminated via a 16-cell thick perfectly matched layer (PML), extended in graphene to drastically attenuate surface waves [10]. In this context, the results are depicted in Fig. 5, proving a remarkable accuracy, especially beyond 10 THz, where the interband term dominates. Moreover, the electric field distribution is illustrated in Fig. 6 for the xy -plane at the $z = 0$ point, where a z -axis oriented dipole source is placed. Th specific cross-section is selected since it highlights that the SPP wavelength is considerably decreased at 20 THz, whereas the propagation length is drastically reduced as computed in Fig. 5. Also, the surface wave is absent at 50 THz, because graphene behaves like a pure conductive layer.

Lastly, the efficiency of the proposed methodology is considered through the comparison with a typical, graphene-free, FDTD code. Obviously, the required memory and CPU time are increased, yet only by a slight percentage, namely, 1.3% and 0.9%, proving that the performance of the FDTD method is effectively retained.

IV. CONCLUSION

The interband conductivity of graphene has been modeled efficiently in this paper via a robust vector-fitting technique for its time-domain numerical representation. The significance

of the interband contribution in the total surface conductivity has been, firstly, evaluated. Then, the vector-fitting approximation has been applied, leading to pairs of complex-conjugate Debye-like terms. Finally, an appropriate algebraic manipulation facilitated the elimination of the complex values, while the symmetry of the complex-conjugate pairs has been exploited to minimize the required surface current terms. The proposed algorithm has been verified successfully through the comparison of the numerically computed SPP characteristics to their corresponding theoretically-derived outcomes.

ACKNOWLEDGMENT

This research is co-financed by Greece and the European Union (European Social Fund- ESF) through the Operational Programme «Human Resources Development, Education and Lifelong Learning» in the context of the project “Reinforcement of Postdoctoral Researchers - 2nd Cycle” (MIS-5033021), implemented by the State Scholarships Foundation (IKY).



REFERENCES

- [1] T. S. Rappaport, Y. Xing, O. Kanhere, S. Ju, A. Madanayake, S. Mandal, A. Alkhateeb, and G. C. Trichopoulos, “Wireless communications and applications above 100 GHz: Opportunities and challenges for 6G and beyond,” *IEEE Access*, vol. 7, pp. 78 729–78 757, 2019.
- [2] A. Singh, M. Andreello, N. Thawdar, and J. M. Jornet, “Design and operation of a graphene-based plasmonic nano-antenna array for communication in the terahertz band,” *IEEE J. Sel. Areas Commun.*, vol. 38, no. 9, pp. 2104–2117, 2020.
- [3] S. Rakheja, P. Sengupta, and S. M. Shakiah, “Design and circuit modeling of graphene plasmonic nanoantennas,” *IEEE Access*, vol. 8, pp. 129 562–129 575, 2020.
- [4] S. Dash, G. Soni, A. Patnaik, C. Liaskos, A. Pitsillides, and I. F. Akyildiz, “Switched-beam graphene plasmonic nanoantenna in the terahertz wave region,” *Plasmonics*, vol. 16, no. 5, pp. 1855–1864, 2021.
- [5] S. Naghizade and H. Saghaei, “Tunable graphene-on-insulator band-stop filter at the mid-infrared region,” *Opt. Quantum Electron.*, vol. 52, no. 4, pp. 1–13, 2020.
- [6] W. Huang, X. Luo, Y. Lu, F. Hu, and G. Li, “Ultra-broadband terahertz bandpass filter with dynamically tunable attenuation based on a graphene–metal hybrid metasurface,” *Appl. Optics*, vol. 60, no. 22, pp. 6366–6370, 2021.
- [7] G. D. Bouzianas, N. V. Kantartzis, T. V. Yioultis, and T. D. Tsioubkis, “Consistent study of graphene structures through the direct incorporation of surface conductivity,” *IEEE Trans. Magn.*, vol. 50, no. 2, pp. 161–164, 2014.
- [8] V. Nayyeri, M. Soleimani, and O. M. Ramahi, “Modeling graphene in the finite-difference time-domain method using a surface boundary condition,” *IEEE Trans. Antennas Propag.*, vol. 61, no. 8, pp. 4176–4182, 2013.
- [9] A. Mock, “Padé approximant spectral fit for FDTD simulation of graphene in the near infrared,” *Opt. Mat. Express*, vol. 2, no. 6, pp. 771–781, 2012.
- [10] S. A. Amanatiadis, T. T. Zygidis, T. Ohtani, Y. Kanai, and N. V. Kantartzis, “A consistent scheme for the precise FDTD modeling of the graphene interband contribution,” *IEEE Trans. Magn.*, vol. 57, no. 6, pp. 1 600 104(1–4), 2021.
- [11] H. Lin, M. F. Pantoja, L. D. Angulo, J. Alvarez, R. G. Martin, and S. G. Garcia, “FDTD modeling of graphene devices using complex conjugate dispersion material model,” *IEEE Microw. Wireless Compon. Lett.*, vol. 22, no. 12, pp. 612–614, 2012.
- [12] G. W. Hanson, “Dyadic Green’s functions for an anisotropic, non-local model of biased graphene,” *IEEE Trans. Antennas Propag.*, vol. 56, no. 3, pp. 747–757, 2008.
- [13] B. Gustavsen and A. Semlyen, “Rational approximation of frequency domain responses by vector fitting,” *IEEE Trans. Power Deliv.*, vol. 14, no. 3, pp. 1052–1061, 1999.